Clusterization and localization of multi-Λ hyperisotopes

Xin Li [1], C. F. Chen [2,*], Xian-Rong Zhou [1,†], and Zhongzhou Ren [2,‡]
[1]*Department of Physics, East China Normal University, Shanghai 200241, China*
[2]*School of Physics Science and Engineering, Tongji University, Shanghai 200092, China*

(Received 1 February 2024; accepted 2 May 2024; published 3 June 2024)

The influence of hyperons on localized clusters is studied in deformed nuclei ^{20}Ne and ^{28}Si and the spherical nucleus ^{40}Ca by employing the deformed Skyrme-Hartree-Fock approach and the localization function. It is found that hyperons in the p state initially tend to occupy the orbitals with shapes similar to that of the core nucleus. The nucleus ^{20}Ne exhibits a robust prolate configuration characterized by an $\alpha - ^{12}\mathrm{C} - \alpha$ cluster, while ^{28}Si displays a less pronounced oblate ringlike cluster. A spherical shell-like cluster structure is possessed by the nucleus ^{40}Ca, and this spherical shape is also maintained in its hyperisotopes. For $^{28}_{8\Lambda}$Ne, the cluster structure retains sufficient strength to maintain its prolate shape even with an enhanced hyperon-nucleon (YN) interaction. In contrast, the cluster structure of $^{36}_{8\Lambda}$Si is comparatively weak, and only a slight enhancement of the YN interaction leads to its cluster structure and deformation collapse.

DOI: 10.1103/PhysRevC.109.064301

I. INTRODUCTION

The clusterization of nuclei is an intriguing phenomenon that has attracted significant attention in both theoretical and experimental fields [1–4]. The most widely investigated cluster is the α particle [5]. Unstable nuclei in the heavy region tend to undergo α decay, indicating the existence of α particles within these nuclei. Due to the relatively small number of nucleons in light nuclei, the occurrence of localized structures can significantly influence their shape and the other properties [6–11]. Therefore, the research on the clusterization in light- and medium-mass regions provides a novel perspective to understanding nuclear shape.

As an important issue for nuclear physics, the mechanism of cluster formation in nuclei has been extensively investigated. The majority of theoretical research aimed at quantitatively describing cluster structures often relies on the α *priori* assumption regarding the existence of such structures [12–15]. It is common to construct Gaussian wave functions centered at given positions in space and the effective interactions are adjusted to reproduce the binding energies and scattering phase shifts associated with these configurations [16,17]. However, the cluster and similar models are constrained by their initial assumptions about the existence of clusters and many shell-model configurations are beyond their reach [18].

The energy density functional theory (EDFT) provides an alternative approach to describe cluster configurations [11,19–21]. Unlike other cluster models, this framework does not presume the existence of cluster structures, but both cluster and mean-field-type states are allowed to be treated simultaneously. A notable advantage of EDFT is its ability to describe a global characterization of cluster states in nuclei, where these states have a simple interpretation in terms of quasimolecular states within this framework [22]. The nuclear structure calculations based on independent-particle density functionals manifest the cluster substructure as marked concentrations of density within the overall total nuclear mass density [5,7,23,24]. However, dealing with the entanglement of these substructures in single-particle orbitals is challenging, since Hartree-Fock single-particle states are usually delocalized and distributed throughout a nucleus. Furthermore, identifying clusters and shell structures based on mass density may be oversimplified because it ignores other aspects of the many-body system.

To provide a more detailed understanding of the underlying structure, Reinhard and collaborators introduced the concept of the localization function into nuclear physics [25], which was originally developed for electronic calculations [26–29]. This function is based on the inverse of the conditional probability of finding a fermion of type q ($= n$, p, or Λ) in the vicinity of another fermion of the same type and with the same spin or signature quantum number σ ($\uparrow$ and $\downarrow$), given that the latter particle is located at position r [30]. The nucleon localization function serves as an excellent tool to reveal shell and cluster effects in nuclei due to its negligible computational cost and its ability to provide a spatial coordinate function to determine the locations of α particles [22,31–33].

In recent years, an increasing number of studies have revealed that α clustering significantly influences the structure of lighter nuclei, such as cluster-nucleon correlations of ^{9}B [34], α-cluster structures of Be [35–37], isoscalar dipole excitations in ^{16}O [15], and the $\alpha + ^{16}$O cluster structure of ^{20}Ne [14]. In addition to the existence of clusters in nuclei, clusters also exist in hypernuclei. The multi-Λ systems involving more than two Λ particles are particularly intriguing. In this case, the Λ hyperon is not merely considered as a minor "impurity," but rather as a third constituent of the

*cfchen@tongji.edu.cn
†xrzhou@phy.ecnu.edu.cn
‡zzren@tongji.edu.cn

nuclear many-body system, giving another dimension to the nuclear chart [38–42]. The clusters of hypernuclei have been discussed in some theoretical calculations [43–47]. Hiyama investigated the clustering structure of the double-Λ hypernucleus ${}^{11}_{\Lambda\Lambda}$Be within the framework of the $\alpha\alpha+\Lambda+\Lambda+n$ five-body cluster model [46]. The light double-Λ hypernucleus ${}^{6}_{\Lambda\Lambda}$He has been studied as a three-body $\Lambda\Lambda\alpha$-cluster system in halo/cluster effective field theory at the leading order, and it has been found that the $\Lambda\Lambda d$ in the spin-0 channel does not exhibit a limit cycle whereas the $\Lambda\Lambda d$ system in the spin-1 channel and the $\Lambda\Lambda\alpha$ system in the spin-0 channel do [47]. In Ref. [44], it was demonstrated that Λ hyperons in ${}^{12}_{4\Lambda}$Be tend to localize around the two α clusters of ^{8}Be. Tanimura conducted a study on deformed multi-Λ hypernuclei using a relativistic mean-field model [48]. It is noteworthy that his calculations did not include ΛΛ pairing correlations.

This study aims to investigate the clustering properties of nuclei and multi-Λ systems within the framework of the Skyrme-Hartree-Fock (SHF) model, incorporating the ΛΛ pairing correlation. Previously, this model has been employed to explore hyperon pairing and deformation in multi-Λ systems [49,50]. However, Ref. [50] primarily focuses on the shape variations of multi-Λ hypernuclei, but it lacks a discussion regarding the internal cluster composition within both the core nuclei and the hypernuclei. Clusterization effects are widely recognized as significant contributors to the structure of $N=Z$ nuclei, leading to a molecular-type phenomenon. This work considers clusters as intrinsic factors in the deformation of both the nuclei and hypernuclei, and it primarily investigates the effects of different numbers of hyperons on the cluster within the hypernuclei. Therefore, ${}^{20+n}_{n\Lambda}$Ne, ${}^{28+n}_{n\Lambda}$Si, and ${}^{40+n}_{n\Lambda}$Ca are selected as the candidate hyperisotope chains, where $n=2$, 4, 6, and 8.

This article is organized as follows. Section II gives a brief introduction to the Skyrme-Hartree-Fock model and the localization measure employed in this work. The results are presented in Sec. III. Finally, the summary and outlook are given in Sec. IV.

II. THEORETICAL FRAMEWORK

A. Skyrme-Hartree-Fock approach

In the framework of the SHF approach, the total energy of a hypernucleus can be written as [51–54]

$$E=\int \mathrm{d}^3\boldsymbol{r}\varepsilon(\boldsymbol{r}),\quad \varepsilon=\varepsilon_{NN}+\varepsilon_{\Lambda N}+\varepsilon_{\Lambda\Lambda}, \tag{1}$$

where ε_{NN}, $\varepsilon_{\Lambda N}$, and $\varepsilon_{\Lambda\Lambda}$ account for the nucleon-nucleon, hyperon-nucleon, and hyperon-hyperon interactions, respectively. The energy density functional depends on the one-body density $\rho_q(\boldsymbol{r})$, the kinetic density $\tau_q(\boldsymbol{r})$, and the spin-orbit current $\boldsymbol{J}_q(\boldsymbol{r})$,

$$\rho_q(\boldsymbol{r})=\sum_{i=1}^{N_q} n_q^i\left|\phi_q^i(\boldsymbol{r})\right|^2,\quad \tau_q(\boldsymbol{r})=\sum_{i=1}^{N_q} n_q^i\left|\nabla\phi_q^i(\boldsymbol{r})\right|^2,$$
$$\boldsymbol{J}_q(\boldsymbol{r})=\sum_{i=1}^{N_q} n_q^i\phi_q^{i*}\left(\nabla\phi_q^i(\boldsymbol{r})\times\sigma\right)/i, \tag{2}$$

where ϕ_q^i $(i=1,\ldots,N_q)$ are the self-consistently calculated single-particle wave functions of the N_q occupied states for the different particles $q=n$, p, and Λ. They satisfy the Schrödinger equation, which is derived by the minimizing of the total energy functional in Eq. (1) according to the variational principle,

$$\left[\nabla\cdot\frac{1}{2m_q^*(\boldsymbol{r})}\nabla-V_q(\boldsymbol{r})+i\boldsymbol{W}_q(\boldsymbol{r})\cdot(\nabla\times\boldsymbol{\sigma})\right]\phi_q^i(\boldsymbol{r})$$
$$=e_q^i\phi_q^i(\boldsymbol{r}), \tag{3}$$

in which $\boldsymbol{W}_q(\boldsymbol{r})$ is the spin-orbit interaction part for the nucleons as given in Ref. [41], while the spin-orbit force for the Λ hyperon is very small [55–57] and it is ignored in the present study. The central mean-fields $V_q(\boldsymbol{r})$, which are corrected by the effective-mass terms following the procedure described in Refs. [53,54], are denoted as

$$V_N=V_N^{\mathrm{SHF}}+\frac{\partial\varepsilon_{N\Lambda}}{\partial\rho_N}$$
$$+\frac{\partial}{\partial\rho_N}\left(\frac{m_\Lambda}{m_\Lambda^*(\rho_N)}\right)\left(\frac{\tau_\Lambda}{2m_\Lambda}-\frac{3}{5}\frac{\rho_\Lambda\left(3\pi^2\rho_\Lambda\right)^{2/3}}{2m_\Lambda}\right), \tag{4}$$

$$V_\Lambda=\frac{\partial(\varepsilon_{N\Lambda}+\varepsilon_{\Lambda\Lambda})}{\partial\rho_\Lambda}-\left(\frac{m_\Lambda}{m_\Lambda^*(\rho_N)}-1\right)\frac{\left(3\pi^2\rho_\Lambda\right)^{2/3}}{2m_\Lambda}. \tag{5}$$

For the nucleonic part ε_{NN}, we employ the Skyrme forces SLy5 [58] and SkI4 [59], which are fitted in a wide nuclear region. The hyperonic parts $\varepsilon_{N\Lambda}$ [54,60] and $\varepsilon_{\Lambda\Lambda}$ [41] are parametrized as (densities ρ given in units of fm^{-3}, energy density ε in MeV fm^{-3}):

$$\varepsilon_{N\Lambda}(\rho_N,\rho_\Lambda)=-\left(\varepsilon_1-\varepsilon_2\rho_N+\varepsilon_3\rho_N^2\right)\rho_N\rho_\Lambda$$
$$+\left(\varepsilon_4-\varepsilon_5\rho_N+\varepsilon_6\rho_N^2\right)\rho_N{\rho_\Lambda}^{5/3}, \tag{6}$$

$$\varepsilon_{\Lambda\Lambda}(\rho_\Lambda)=-\varepsilon_7\rho_\Lambda^2\Theta(N_\Lambda>1), \tag{7}$$

together with

$$\frac{m_\Lambda^*}{m_\Lambda}(\rho_N)\approx\mu_1-\mu_2\rho_N+\mu_3\rho_N^2-\mu_4\rho_N^3. \tag{8}$$

The parameters $\varepsilon_1,\ldots,\varepsilon_6$ in Eq. (6) and the Λ effective-mass μ_i in Eq. (8) were obtained by performing BHF calculations on hypernuclear bulk matter with the Nijmegen potential NSC97f [54,60], while the empirical expression parameter ε_7 (labeled EmpC) has been determined by fitting the bound energy of ${}^{6}_{\Lambda\Lambda}$He in the Ref. [41].

The occupation probabilities n_q^i for nucleons in Eq. (2) are determined by the inclusion of pairing effects within a BCS approximation. In this study, the pairing interaction is taken as a density-dependent δ interaction [61],

$$V_q(\boldsymbol{r}_1,\boldsymbol{r}_2)=V_0^{(q)}\left[1-\frac{\rho_{N(\Lambda)}[(\boldsymbol{r}_1+\boldsymbol{r}_2)/2]}{0.16\ \mathrm{fm}^{-3}}\right]\delta(\boldsymbol{r}_1-\boldsymbol{r}_2), \tag{9}$$

with the pairing strength $V_0^{(N)}=-1000$ MeV fm^3 for both neutrons and protons as in Ref. [62].

Although Ref. [42] indicates that the ΛΛ pairing effect can generally be neglected in most hypernuclei, it must be emphasized that the ΛΛ pairing should be taken into account

in the hypernuclei under examination in our study, as they involve a significant number of hyperons. For Λ hyperons, we take the strength of the pairing interaction $V_0^{(\Lambda)}$ as 4/9 of that for nucleons [42,49].

In our approach, we assume the axial symmetry of the mean field and solve the deformed SHF Schrödinger equation using cylindrical coordinates (r, z) within the axially deformed harmonic-oscillator basis [63]. The geometric quadrupole deformation parameter of the nuclear core is expressed as

$$\beta_2 \equiv \frac{4\pi}{5A}\frac{\int d^3r r^2 Y_{20}\rho}{(0.93A^{1/3})^2}, \tag{10}$$

where A is the number of nucleons and $0.93A^{1/3}$ is the average radius of the corresponding nucleus.

B. Localization function

The localization measure was originally introduced in atomic and molecular physics to characterize chemical bonds in electronic systems [28,29,64] and was subsequently introduced to nuclear systems [25,65,66]. The localization function is related to the spatial two-body correlation between two like-spin fermions of the same kind and can be applied to different fermion systems, including nuclei and hypernuclei [22,48,65,66]. It can be written as the probability of finding the second particle located within a shell of small radius around the assumed particle at r with the same spin σ (↑ and ↓) and isospin q (= n, p, or Λ) [25,64]:

$$R_{q\sigma}(\mathbf{r}, \delta) \approx \frac{1}{3}\left(\tau_{q\sigma} - \frac{1}{4}\frac{[\nabla\rho_{q\sigma}]^2}{\rho_{q\sigma}} - \frac{\boldsymbol{J}_{q\sigma}^2}{\rho_{q\sigma}}\right)\delta^2 + \mathcal{O}(\delta^3), \tag{11}$$

where the particle density $\rho_{q\sigma}$, the kinetic energy density $\tau_{q\sigma}$, and the current density $\boldsymbol{J}_{q\sigma}$ can be referred in Eq. (2) with spin σ, and the density gradient $\nabla\rho_{q\sigma}$ is given by

$$\nabla\rho_{q\sigma}(\boldsymbol{r}) = 2\sum_{i=1}^{N_q} n_q^i \,\mathrm{Re}\left[\phi_q^{i*}(\boldsymbol{r})\nabla\phi_q^i(\boldsymbol{r})\right]. \tag{12}$$

The expression shown in Eq. (11) can serve as the definition of a localization measure,

$$D_{q\sigma}(\mathbf{r}) = \left(\tau_{q\sigma} - \frac{1}{4}\frac{[\nabla\rho_{q\sigma}]^2}{\rho_{q\sigma}} - \frac{\boldsymbol{J}_{q\sigma}^2}{\rho_{q\sigma}}\right). \tag{13}$$

However, the localization measure defined by Eq. (13) is a reverse relation, and it is customary to define a reverse-normalized localized measure [25],

$$\mathcal{C}_{q\sigma}(\boldsymbol{r}) = \left[1 + \left(\frac{\rho_{q\sigma}\tau_{q\sigma} - \boldsymbol{j}_{q\sigma}^2 - \frac{1}{4}[\nabla\rho_{q\sigma}]^2}{\rho_{q\sigma}\tau_{q\sigma}^{\mathrm{TF}}}\right)^2\right]^{-1}, \tag{14}$$

where $\tau_{q\sigma}^{\mathrm{TF}} = \frac{3}{5}(6\pi^2)^{2/3}\rho_{q\sigma}^{5/3}$ is the Thomas-Fermi kinetic energy density.

For a more detailed discussion on the physical meaning of the localization function can be found in Refs. [25,66]. We focus on $\mathcal{C}_{q\sigma}(\boldsymbol{r}) \approx 1$ for all nucleonic states $(q\sigma) = (n\uparrow, n\downarrow, p\uparrow, p\downarrow, \Lambda\uparrow, \Lambda\downarrow)$, indicating a complete overlap of the four nucleons. This implies a significant localization of an α cluster at the designated position. It should be noted that $\mathcal{C}_{q\sigma}(\boldsymbol{r}) \approx 1$ simultaneously for all the spin-isospin combinations is a minimal necessary condition of α clusterization [25]. This feature is calculated at the mean-field level without α *priori* assumption. Owing to the minor distinctions between bound and free α particles within atomic nuclei, $\mathcal{C}_{q\sigma}$ can be interpreted as a quantitative measure representing the extent of localization within atomic nuclei.

III. RESULTS AND DISCUSSION

In general, the deformation of both nuclei and hypernuclei can be explained by considering the single-particle energy levels occupied by nucleons close to the Fermi surface. Furthermore, the energy density functional method provides an understanding of this phenomenon by utilizing the nucleon density distribution. However, the nucleon density distribution is the result of the accumulation of all occupied single-particle energy levels, and thus it loses much more detailed information. In this paper, we utilize the localization function to provide a more comprehensive analysis of the nuclear localization structure. For light $N = Z$ even-even nuclei, the localization distributions of protons $(\mathcal{C}_p)$ and neutrons $(\mathcal{C}_n)$, as well as spin-up $(\mathcal{C}_\uparrow)$ and spin-down $(\mathcal{C}_\downarrow)$ states, exhibit considerable similarity due to the small Coulomb interaction and fully occupied single-particle energy levels. Consequently, a singular parameter, $\mathcal{C}_{p\uparrow}$, adequately describes all previously mentioned parameters including $\mathcal{C}_{p\uparrow}$, $\mathcal{C}_{p\downarrow}$, $\mathcal{C}_{n\uparrow}$, and $\mathcal{C}_{n\downarrow}$.

Due to the above convenience, the current study utilizes the localization distribution of spin-up neutrons $\mathcal{C}_{n\uparrow}$ as their nucleon localization distribution $\mathcal{C}$ to investigate the structure of localized clusters in ^{16}O, ^{20}Ne, ^{28}Si, and ^{40}Ca. The density distributions of these nuclei and their corresponding hyperisotopes are calculated using the deformed Skyrme-Hartree-Fock + BCS formalism with the NSC97f ΛN parameter [54,60].

Figure 1 illustrates a cut through the profile of the density and localization function. As mentioned in Ref. [67], the density distribution of ^{16}O displays a dip at its center, which may not be readily discernible in the density distribution due to the consistently high density at the nucleus center, and it becomes significantly pronounced in the localization distribution. Notably, the results with different parameters (SkI4 and SLy5) demonstrate a high degree of consistency, indicating the robustness of the localization distribution. To facilitate subsequent calculations, we adopt the SkI4 parameter.

To comprehensively explore the impurity effects of multi-Λ in different nuclei, we have selected three nuclei with distinct stable shapes as candidate cores: prolate ^{20}Ne, oblate ^{28}Si, and spherical ^{40}Ca. The distributions of the localization function and the density for the ground state of each core are presented in Fig. 2. The upper panels display the localization distributions $\mathcal{C}$, while the lower panels illustrate the corresponding neutron density distributions ρ. For ^{20}Ne, two regions with high localization are evident at the outer ends of the symmetry z axis, accompanied by a slightly enhanced localization ring at the central position along the r axis. This can be interpreted as a quasimolecular $\alpha - ^{12}\mathrm{C} - \alpha$ configuration, consistent with the relativistic mean-field studies [48,68]. It

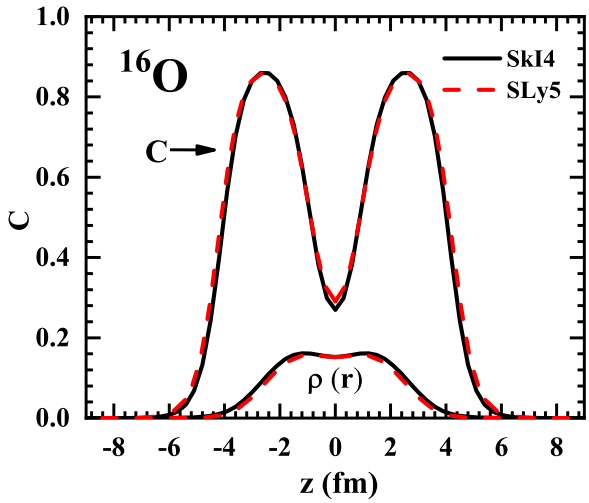

FIG. 1. The nucleon density and localization function distributions of the ^{16}O nucleus are presented with different interaction parameters SkI4 and SLy5, respectively. Different interaction parameters give similar density and localization distributions. The localization distribution provides a clearer depiction of the internal structure of ^{16}O and more distinctly reveals the dip at the center of ^{16}O compared to the density distribution.

is notable that studies emphasizing cluster structure suggest that ^{20}Ne exhibits an asymmetric cluster structure associated with $\alpha + {}^{16}$O [69,70]. In this work, we employ the mean-field method to obtain the density distributions of nuclei and hypernuclei by considering only quadrupole deformation, without any α priori assumption. Taking into account the octupole deformation of the $\alpha + {}^{16}$O configuration effectively reproduces the negative-parity bands of ^{20}Ne and offers better corrections for its positive-parity bands. However, focusing solely on quadrupole deformation projection still yields a satisfactory positive-parity band, indicating an underlying $\alpha + {}^{12}\mathrm{C} + \alpha$ structure [71].

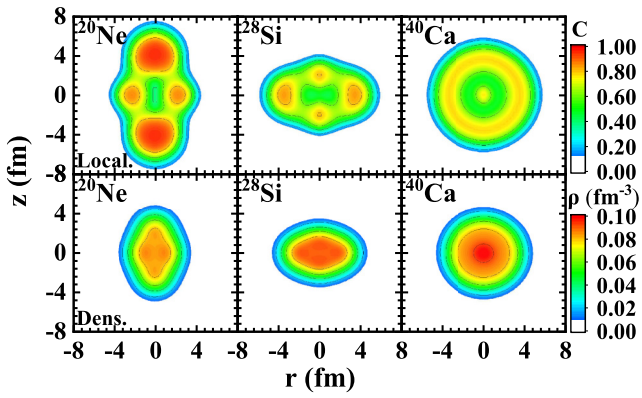

FIG. 2. Color map plots depicting the localization (upper panel) and neutron density (lower panel, in fm^{-3}) distributions for $Z = N$ nuclei ^{20}Ne, ^{28}Si, and ^{40}Ca, respectively. The prolate deformed $\alpha - {}^{12}\mathrm{C} - \alpha$ structure of ^{20}Ne, the oblate deformed ringlike cluster of ^{28}Si, and the spherical shell-like cluster of ^{40}Ca are presented.

In cases where maximum values of $\mathcal{C}$ deviate from the symmetry axis, as observed in ^{28}Si, our computational results indicate the existence of a ringlike distribution of localized structures on the nuclear surface, characterized by axial symmetry around the z axis. For the closed-shell nucleus ^{40}Ca, the distribution of its localization structures exhibits a layered shell-like pattern. Although a small region in the central area exhibits the characteristics of clusterization, its extent is significantly smaller than the radius of an α particle ($\approx$1.7 fm). Therefore, it can be inferred that the cluster structure of ^{40}Ca is predominantly concentrated on its surface. The nucleon density and localization function distributions of ^{28}Si and ^{40}Ca imply that the nucleonic cluster configuration in these nuclei does not manifest as localized α clusters. Instead, it demonstrates a nonlocalized cluster arrangement distributed across the region with maximum radius on the surface. The comparatively weaker cluster structure observed in ^{28}Si may potentially account for its softer deformation in intrinsic states. Nevertheless, it is crucial to acknowledge that this explanation is speculative, and further theoretical investigations are necessary to validate this assumption. It is evident that the structural arrangements of the localized function $\mathcal{C}$, whether in the form of α clusters or nonlocalized cluster structures, provide a more intuitive depiction of information compared to its density distribution. In previous studies, the exploration of impurity effects induced by hyperons primarily concentrated on assessing their influence on the core nucleus. However, a single-hyperon hypernucleus does not provide an ideal target to investigate the influences of hyperons on the core nuclei. This limitation arises from the significant disparity between the number of hyperons and nucleons present. They give rise to minimal shape modifications and influences, comparable to the effects caused by hyperons themselves, let alone their impact on the cluster structure of core nuclei. Furthermore, it has been observed that the presence of multiple hyperons results in a more diverse array of impurity effects. This phenomenon is not only associated with the deformation of the nucleus but also relies on the single-particle orbitals occupied by hyperons. Therefore, the research presented in this paper is dedicated to analyzing the impurity effects of hyperons in multi-Λ hyperisotopes.

The density distributions of the lowest s and p single-particle orbitals, occupied by Λ hyperons, are shown in Fig. 3, where ${}^{48}_{8\Lambda}$Ca is employed as an example. Due to the negligible contribution of the spin-orbit force for Λ hyperons, the two oblate deformed [101] orbitals are degenerate, with only the [110] orbital exhibiting prolate deformation. The strength of the hyperon-nucleon interaction potential is determined by the degree of density overlap. Consequently, the filling sequence of p orbitals for hyperons varies based on the distinct ground-state shapes of hypernuclei. In particular, the [101] orbital exhibits lower energy in oblate deformation, whereas the [110] orbital displays lower energy in the case of prolate deformation. This shape-dependent filling order of hyperon orbitals results in diverse trends in the morphological variations of multi-Λ hypernuclei.

The density distributions of nucleons and Λ hyperons in hyperisotopes characterized by distinct ground-state shapes, namely, prolate ^{20}Ne, oblate ^{28}Si, and spherical ^{40}Ca, are

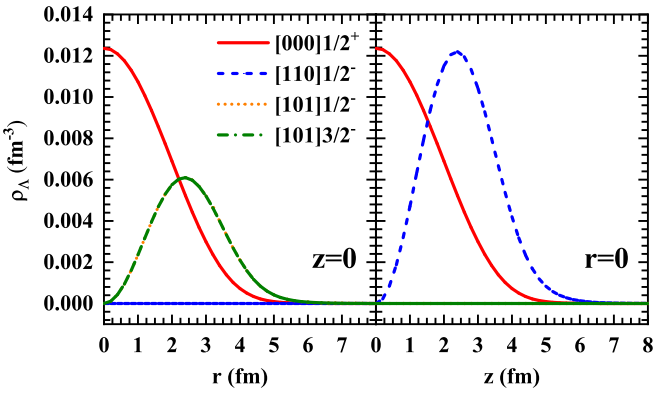

FIG. 3. Density distributions for the occupied s and p single-particle orbitals of Λ hyperons in $^{48}_{8\Lambda}$Ca at $\beta_2 = 0$ as functions of r ($z = 0$) and z ($r = 0$). The z axis is the symmetry axis. The spin-orbit force of Λ hyperons is small to neglected; therefore, the two oblate [101] orbitals are degenerate and only one prolate [110] orbital exists.

illustrated in Fig. 4. The ground state of ^{20}Ne displays a distinct prolate deformation, and the introduction of hyperons results in notable modifications in the density distribution within the cores of the corresponding hyperisotopes. Furthermore, it is noteworthy that the shape of hyperons in these

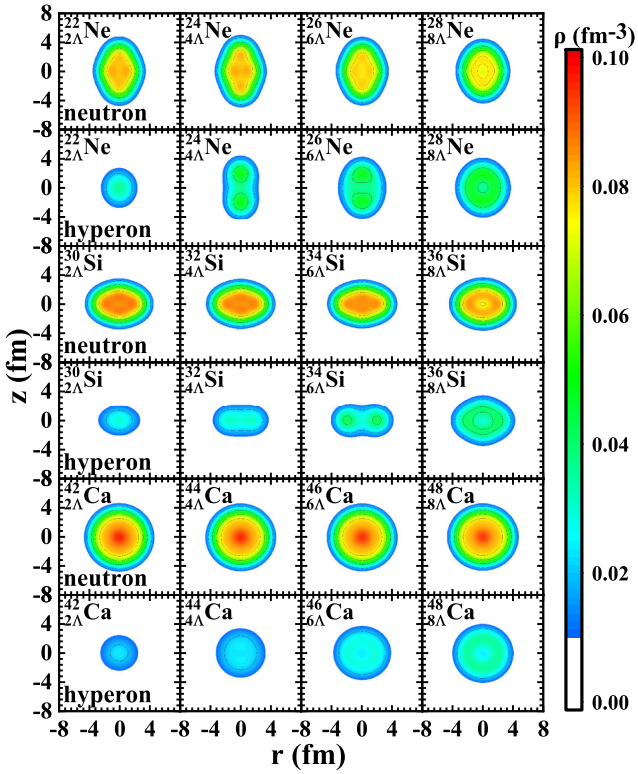

FIG. 4. The density distributions of neutrons and hyperons on the zr plane in the Ne, Si, and Ca hyperisotopes, respectively. Hyperons in the p orbitals tend to initially fill orbitals with a shape similar to that of the core nuclei, thereby enhancing the prolate deformation in $^{24}_{4\Lambda}$Ne and the oblate deformation in $^{32}_{2\Lambda}$Si and $^{34}_{4\Lambda}$Si.

hyperisotopes is heavily influenced by the initial prolate shape of ^{20}Ne. In the double-Λ hypernucleus $^{20}_{2\Lambda}$Ne, the density of hyperons reflects the deformation of the core, as the two additional hyperons occupy the spherical orbital $[000]1/2^+$. Upon adding 4Λ hyperons, there is a discernible tendency for the hyperons to favor a specific shape of p orbital, which is strongly influenced by the deformation of the core. Due to the prolate deformation of ^{20}Ne, the hyperons are initially filled in the prolate $[110]1/2^-$ orbital. With the introduction of more hyperons, they occupy the two degenerate oblate orbitals $[101]1/2^-$ and $[101]3/2^-$. Hence, $^{24}_{4\Lambda}$Ne exhibits the highest degree of deformation among its hyperisotopes. Nevertheless, with the addition of more Λ hyperons, the occupation of oblate orbitals contributes to a reduction in the degree of deformation. When the hyperon count in $^{28}_{8\Lambda}$Ne reaches eight, the distribution of hyperons transitions back to a spherical shape.

For the hyperisotopes corresponding to ^{28}Si and ^{40}Ca, the filling order of hyperon orbitals and their respective shape modification effects are distinct. In ^{28}Si hyperisotopes with oblate deformation, the hyperons initially occupy the two degenerate oblate [101] orbitals. Therefore, the deformation can be increased until accommodating 6Λ hyperons, at which the maximum deformation is reached. Then hyperons will fill into the prolate [110] orbital, causing a reduction of the deformation. However, in the spherical hyperisotopes corresponding to ^{40}Ca, Λ hyperons do not exhibit any preference for oblate or prolate p orbits. As a consequence, the shape of these hypernuclei remains spherical throughout the entire hyperisotope range.

In the calculations of multi-Λ hyperisotopes, the ΛΛ pairing correlation is included. However, this correlation becomes ineffective when the hyperon count reaches the magic numbers, and the hyperon pairing gaps are significantly smaller than those of nucleons. In deformed nuclei, the pairing correlation is further weakened. For $^{24}_{4\Lambda}$Ne, the pairing energy of hyperons (1.475 MeV) constitutes less than 10% of the total pairing energy (11.379 MeV). Therefore, although the pairing effect of hyperons is included in our work, it has little effect on the results such as the density distribution of hyperons. Therefore, as described in Ref. [42], the ΛΛ pairing effect can usually be neglected in most hypernuclei, even in hypernuclei with a large numbers of hyperons.

The detailed quadrupole deformation parameters β_2 and root-mean-squared radii $\langle r \rangle$ are listed in Table I. For hypernuclei with two or eight hyperons, it can be seen that the deformation parameter β_2 is smaller than that of their corresponding core nuclei, and the density of hyperons tends to be spherical. The sudden drop of 2Λ separation energies, along with the vanished average pairing gaps and pairing energies, implies $-S = 2$ and $-S = 8$ also serve as the hyperon magic numbers [49]. However, due to the negligible spin-orbit interaction, the hyperon magic numbers differ from conventional nucleon magic numbers, and they also do not inherently imply a spherical shape for hypernuclei. This deviation arises from the weak interaction between hyperons, and the shell formation based on the hyperon magic numbers tends towards a spherical shape due to the complete filling of hyperon orbitals, rather than mutual attraction between hyperons.

TABLE I. Quarupole deformation parameters β_2 and root-mean-squared radii $\langle r\rangle$ of the Ne, Si, and Ca hyperisotopes, where the subscripts N and Λ represent the nucleon and the Λ hyperon, respectively. β_2 is the deformation parameter for all baryons in (hyper)nuclei. N_Λ is the number of Λ hyperons.

	Ne hyperisotopes					Si hyperisotopes					Ca hyperisotopes				
N_Λ	β_{2N}	$\beta_{2\Lambda}$	β_2	$\langle r_N\rangle$	$\langle r_\Lambda\rangle$	β_{2N}	$\beta_{2\Lambda}$	β_2	$\langle r_N\rangle$	$\langle r_\Lambda\rangle$	β_{2N}	$\beta_{2\Lambda}$	β_2	$\langle r_N\rangle$	$\langle r_\Lambda\rangle$
0	0.567		0.567	2.882		−0.484		−0.484	3.155		0.000		0.000	3.329	
2	0.480	0.193	0.454	2.856	2.496	−0.482	−0.244	−0.468	3.152	2.663	0.000	0.000	0.000	3.325	2.788
4	0.603	0.652	0.614	2.884	3.036	−0.488	−0.381	−0.472	3.154	3.098	0.000	0.000	0.000	3.324	3.148
6	0.467	0.266	0.402	2.857	3.170	−0.495	−0.416	−0.477	3.158	3.235	0.000	0.000	0.000	3.323	3.363
8	0.323	0.102	0.236	2.840	3.211	−0.458	−0.155	−0.373	3.141	3.291	0.000	0.000	0.000	3.324	3.321

The main interaction experienced by hyperons comes from the attractive forces exerted by nucleons. Therefore, when the hyperon count reaches the magic numbers, the shape of the hypernuclei remains close to the original shape of the core nuclei.

The ^{20}Ne chain reaches its maximum deformation with 4Λ, while ^{28}Si achieves its maximum with 6Λ. However, it is noteworthy that in the case of $^{36}_{8\Lambda}$Si, despite the hyperon density distribution approaching spherical, it fails to overcome the deformation of neutrons. This differs from the results reported in Ref. [48], where the addition of eight Λ hyperons to ^{28}Si was found to overcome the nucleons' deformation, resulting in a spherical system. The potential energy surface of ^{28}Si is somewhat soft, and one might expect a large harmonic effect of collective vibration [72]. The predicted deformations of the Si hyperisotopes may depend on the model used.

We also examined the localization distributions of nucleons within hypernuclei and found a high degree of consistency with Fig. 2. This observation indicates that although the addition of hyperons to the core does lead to shape modifications, these alterations have minimal impact on the internal cluster structure of the nucleus. To gain deeper insights into the relationship between the cluster structure and the nuclear shape of hypernuclei, we artificially intensified the YN interaction, and the results are shown in Fig. 5. By increasing the interaction strength to 1.12 times its initial value, the cluster structure of $^{36}_{8\Lambda}$Si undergoes a collapse, resulting in a spherical nuclear shape. In contrast, when the interaction strength of Ne is increased to 2 times its original value (a stronger YN interaction strength will lead to a cluster collapse with an unreasonably large nucleon density distribution in the central area), the core nucleus still maintains its original deformed state. This indicates that the cluster structure of ^{20}Ne is highly developed and is resistant to disruption by hyperons. It is well known that a Λ particle reduces the intercluster distance between α and d in ^{6}Li [73–75]. This occurs because, when a Λ hyperon is introduced into a relatively light nucleus like ^{6}Li, it occupies the s-state orbital located at the geometric center. This leads to a pronounced shrinkage effect on the surrounding clusters due to the larger overlap between the hyperon and the cluster. However, in the heavier nucleus ^{20}Ne, which contains numerous nucleons, the shrinkage effect of a single hyperon is limited. Consequently, it is hard for a hyperon to reduce the intercluster distance between α and other nucleons in the nucleus. In the case of $^{28}_{8\Lambda}$Ne, hyperons are not solely concentrated at the geometric center. The distribution range of the hyperons becomes wider due to the attraction of the clusters, and then the shrinkage effect of the hyperons becomes dispersed. Therefore, in nuclei with robust cluster structures, the influence of hyperons is minimal. Conversely, in nuclei with softer potential surfaces, the addition of hyperons can disrupt the cluster structure. The cluster structure of the core nucleus plays a crucial role in maintaining its deformation, and significant changes occur in the shape of the core nucleus when it is completely disrupted.

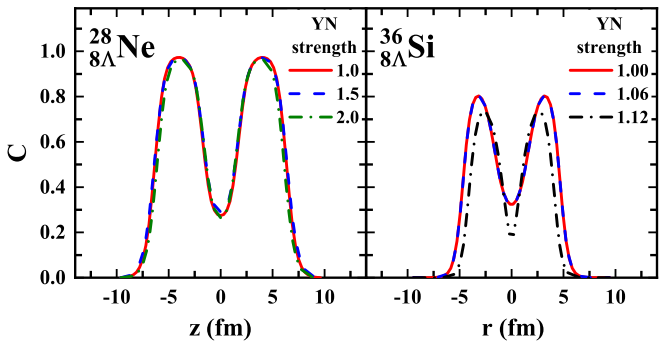

FIG. 5. The localization function distributions for $^{28}_{8\Lambda}$Ne and $^{36}_{8\Lambda}$Si at different YN interaction strengths, respectively. Note that all $^{28}_{8\Lambda}$Ne are prolate deformed, while $^{36}_{8\Lambda}$Si changes from oblate to spherical when the YN interaction strength reaches 1.12.

IV. SUMMARY

Within the framework of the deformed Skyrme-Hartree-Fock + BCS formalism and utilizing the localization function, we investigate the presence of localized clusters in the deformed nuclei ^{20}Ne and ^{28}Si and the spherical nucleus ^{40}Ca. Additionally, we explore the impurity effects of multi-Λ hyperons on their respective hyperisotopes by employing an effective ΛN interaction with modified $\Lambda\Lambda$ interaction considering the impact of $\Lambda\Lambda$ pairing correlations.

The inclusion of 2Λ or 8Λ hyperons generally leads to a decrease in the deformation of the nuclear core, while the presence of 4Λ and 6Λ hyperons enhances nuclear deformation. These phenomena are explained at the microscopic level through an analysis of the density distributions of the occupied Λ_p orbitals. The analysis demonstrates that hyperons in the p state tend to initially occupy orbitals with a shape similar to that of the core nucleus. The nucleus ^{20}Ne exhibits a prolate shape, and in its hyperisotopes, hyperons in the p state

initially occupy the prolate [110] orbital. This occupancy pattern contributes to an increase in the prolate core deformation, reaching its maximum with the addition of 4Λ hyperons. Conversely, the nucleus ^{28}Si displays an oblate shape, and the hyperons are filled into the degenerate pair of oblate [101] orbitals initially, leading to an increase in the oblate core deformation. The maximum degree of deformation is achieved with the introduction of 6Λ hyperons. In contrast, hyperons in the spherical core of ^{40}Ca do not show any preferences for the shape of the p orbitals and maintain a spherical configuration.

The distribution of clusters within the nucleus, as determined by the localization function, provides a more intuitive representation of its shape characteristics compared to the density distribution. This indicates that the shape of the nucleus is primarily influenced by its internal cluster structure. The localization function distribution reveals that ^{20}Ne exhibits two highly localized regions at the outer ends of the symmetry axis, implying an $\alpha - ^{12}\mathrm{C} - \alpha$ configuration. A weak ringlike cluster and a shell-like cluster (not an α cluster) are found in the oblate ^{28}Si and the spherical ^{40}Ca cases, respectively. The presence of clusters plays a crucial role in maintaining the deformation of these nuclei during the addition of Λ hyperons. The cluster structure of $^{28}_{8\Lambda}$Ne exhibits sufficient strength to maintain a prolate shape even under an enhanced YN interaction. Conversely, the cluster structure of $^{36}_{8\Lambda}$Si undergoes collapse and transitions to a spherical shape with only slightly enhancing the YN interaction. Based on comparative analysis, it can be concluded that the strength of clusters within a deformed nucleus indicates the degree of its shape softness or hardness.

ACKNOWLEDGMENT

This work was supported by the National Natural Science Foundation of China under Contracts No. 12175071, No. 12035011, and No. 11975167 and the National Key R&D program of China under Contract No. 2023YFA16065031.

[1] W. von Oertzen, M. Freer, and Y. Kanada-En'yo, Phys. Rep. **432**, 43 (2006).
[2] Z. H. Yang *et al.*, Phys. Rev. Lett. **112**, 162501 (2014).
[3] D. J. Marín-Lámbarri, R. Bijker, M. Freer, M. Gai, T. Kokalova, D. J. Parker, and C. Wheldon, Phys. Rev. Lett. **113**, 012502 (2014).
[4] D. Ray and A. V. Afanasjev, Phys. Rev. C **94**, 014310 (2016).
[5] J. A. Maruhn, M. Kimura, S. Schramm, P.-G. Reinhard, H. Horiuchi, and A. Tohsaki, Phys. Rev. C **74**, 044311 (2006).
[6] J.-P. Ebran, E. Khan, T. Nikšić, and D. Vretenar, Nature (London) **487**, 341 (2012).
[7] Y. Fukuoka, S. Shinohara, Y. Funaki, T. Nakatsukasa, and K. Yabana, Phys. Rev. C **88**, 014321 (2013).
[8] L. Wang, J. Liu, R. Wang, M. Lyu, C. Xu, and Z. Ren, Phys. Rev. C **103**, 054307 (2021).
[9] H. Zhang, D. Bai, Z. Wang, and Z. Ren, Phys. Rev. C **105**, 054317 (2022).
[10] L. Wang, Q. Niu, J. Zhang, J. Liu, and Z. Ren, Sci. China Phys. Mech. Astron. **66**, 102011 (2023).
[11] Z. Yuan, D. Bai, Z. Wng, Z. Ren, and D. Ni, Sci. China Phys. Mech. Astron. **66**, 222012 (2023).
[12] E. Uegaki, Y. Abe, S. Okabe, and H. Tanaka, Prog. Theor. Phys. **62**, 1621 (1979).
[13] M. Chernykh, H. Feldmeier, T. Neff, P. von Neumann-Cosel, and A. Richter, Phys. Rev. Lett. **98**, 032501 (2007).
[14] B. Zhou, Y. Funaki, H. Horiuchi, Z. Ren, G. Röpke, P. Schuck, A. Tohsaki, C. Xu, and T. Yamada, Phys. Rev. Lett. **110**, 262501 (2013).
[15] Y. Kanada-En'yo and Y. Shikata, Phys. Rev. C **100**, 014301 (2019).
[16] H. Feldmeier and J. Schnack, Prog. Part. Nucl. Phys. **39**, 393 (1997).
[17] Y. Kanada-En'yo, M. Kimura, and A. Ono, Prog. Theor. Exp. Phys. **2012**, 01A202 (2012).
[18] A. V. Afanasjev and H. Abusara, Phys. Rev. C **97**, 024329 (2018).
[19] J.-P. Ebran, E. Khan, T. Nikšić, and D. Vretenar, Phys. Rev. C **90**, 054329 (2014).
[20] R. O. Jones, Rev. Mod. Phys. **87**, 897 (2015).
[21] J.-P. Ebran, E. Khan, T. Nikšić, and D. Vretenar, J. Phys. G: Nucl. Part. Phys. **44**, 103001 (2017).
[22] C. L. Zhang, B. Schuetrumpf, and W. Nazarewicz, Phys. Rev. C **94**, 064323 (2016).
[23] S. Takami, K. Yabana, and K. Ikeda, Prog. Theor. Phys. **96**, 407 (1996).
[24] H. Ohta, K. Yabana, and T. Nakatsukasa, Phys. Rev. C **70**, 014301 (2004).
[25] P.-G. Reinhard, J. A. Maruhn, A. S. Umar, and V. E. Oberacker, Phys. Rev. C **83**, 034312 (2011).
[26] A. Savin, R. Nesper, S. Wengert, and T. F. Fässler, Angew. Chem. Int. Ed. Engl. **36**, 1808 (1997).
[27] A. Scemama, P. Chaquin, and M. Caffarel, J. Chem. Phys. **121**, 1725 (2004).
[28] M. Kohout, Int. J. Quantum Chem. **97**, 651 (2004).
[29] T. Burnus, M. A. L. Marques, and E. K. U. Gross, Phys. Rev. A **71**, 010501(R) (2005).
[30] P. Jerabek, B. Schuetrumpf, P. Schwerdtfeger, and W. Nazarewicz, Phys. Rev. Lett. **120**, 053001 (2018).
[31] B. Schuetrumpf and W. Nazarewicz, Phys. Rev. C **96**, 064608 (2017).
[32] F. Mercier, A. Bjelčić, T. Nikšić, J.-P. Ebran, E. Khan, and D. Vretenar, Phys. Rev. C **103**, 024303 (2021).
[33] Z. X. Ren, J. Zhao, D. Vretenar, T. Nikšić, P. W. Zhao, and J. Meng, Phys. Rev. C **105**, 044313 (2022).
[34] Q. Zhao *et al.*, Phys. Rev. C **97**, 054323 (2018).
[35] M. Lyu, Z. Ren, B. Zhou, Y. Funaki, H. Horiuchi, G. Röpke, P. Schuck, A. Tohsaki, C. Xu, and T. Yamada, Phys. Rev. C **93**, 054308 (2016).
[36] D. Bai and Z. Ren, Phys. Rev. C **101**, 034311 (2020).
[37] D. Bai and Z. Ren, Phys. Rev. C **103**, 044316 (2021).
[38] J. Schaffner, C. Greiner, and H. Stöcker, Phys. Rev. C **46**, 322 (1992).
[39] J. Schaffner, C. B. Dover, A. Gal, C. Greiner, D. J. Millener, and H. Stöcker, Ann. Phys. **235**, 35 (1994).
[40] E. Khan, J. Margueron, F. Gulminelli, and A. R. Raduta, Phys. Rev. C **92**, 044313 (2015).

[41] J. Margueron, E. Khan, and F. Gulminelli, Phys. Rev. C **96**, 054317 (2017).
[42] H. Güven, K. Bozkurt, E. Khan, and J. Margueron, Phys. Rev. C **98**, 014318 (2018).
[43] H. Bandō, K. Ikeda, and T. Motoba, Prog. Theor. Phys. **66**, 1344 (1981).
[44] K. Miyahara, K. Ikeda, and H. Bandō, Prog. Theor. Phys. **69**, 1717 (1983).
[45] K. Ikeda, H. Bandō, and T. Motoba, Prog. Theor. Phys. Suppl. **81**, 147 (1985).
[46] E. Hiyama, J. Phys.: Conf. Ser. **436**, 012080 (2013).
[47] S.-I. Ando, Int. J. Mod. Phys. E **25**, 1641005 (2016).
[48] Y. Tanimura, Phys. Rev. C **99**, 034324 (2019).
[49] J. Guo, C. F. Chen, X.-R. Zhou, Q. B. Chen, and H.-J. Schulze, Phys. Rev. C **105**, 034322 (2022).
[50] C. F. Chen, Q. B. Chen, X.-R. Zhou, Y. Y. Cheng, J.-W. Cui, and H.-J. Schulze, Chin. Phys. C **46**, 064109 (2022).
[51] M. Rayet, Nucl. Phys. A **367**, 381 (1981).
[52] J. Cugnon, A. Lejeune, and H.-J. Schulze, Phys. Rev. C **62**, 064308 (2000).
[53] X.-R. Zhou, H.-J. Schulze, H. Sagawa, C.-X. Wu, and E.-G. Zhao, Phys. Rev. C **76**, 034312 (2007).
[54] H.-J. Schulze and T. Rijken, Phys. Rev. C **88**, 024322 (2013).
[55] W. Brückner *et al.*, Phys. Lett. B **79**, 157 (1978).
[56] S. Ajimura *et al.*, Phys. Rev. Lett. **86**, 4255 (2001).
[57] Y. Zhang, H. Sagawa, and E. Hiyama, Phys. Rev. C **103**, 034321 (2021).
[58] E. Chabanat, P. Bonche, P. Haensel, J. Meyer, and R. Schaeffer, Nucl. Phys. A **635**, 231 (1998).
[59] P.-G. Reinhard and H. Flocard, Nucl. Phys. A **584**, 467 (1995).
[60] I. Vidaña, A. Polls, A. Ramos, and H.-J. Schulze, Phys. Rev. C **64**, 044301 (2001).
[61] N. Tajima, P. Bonche, H. Flocard, P.-H. Heenen, and M. S. Weiss, Nucl. Phys. A **551**, 434 (1993).
[62] M. T. Win, K. Hagino, and T. Koike, Phys. Rev. C **83**, 014301 (2011).
[63] D. Vautherin, Phys. Rev. C **7**, 296 (1973).
[64] A. D. Becke and K. E. Edgecombe, J. Chem. Phys. **92**, 5397 (1990).
[65] J.-P. Ebran, E. Khan, T. Nikšić, and D. Vretenar, Phys. Rev. C **87**, 044307 (2013).
[66] E. Khan, L. Heitz, F. Mercier, and J.-P. Ebran, Phys. Rev. C **106**, 064330 (2022).
[67] J. Friedrich and N. Voegler, Nucl. Phys. A **373**, 192 (1982).
[68] J.-P. Ebran, E. Khan, T. Nikšić, and D. Vretenar, Phys. Rev. C **89**, 031303(R) (2014).
[69] Y. Kanada-En'yo and K. Ogata, Phys. Rev. C **101**, 064308 (2020).
[70] B. Zhou, Y. Funaki, H. Horiuchi, Y.-G. Ma, G. Röpke, P. Schuck, A. Tohsaki, and T. Yamada, Nat. Commun. **14**, 8206 (2023).
[71] E. F. Zhou, J. M. Yao, Z. P. Li, J. Meng, and P. Ring, Phys. Lett. B **753**, 227 (2016).
[72] M. T. Win and K. Hagino, Phys. Rev. C **78**, 054311 (2008).
[73] E. Hiyama, M. Kamimura, K. Miyazaki, and T. Motoba, Phys. Rev. C **59**, 2351 (1999).
[74] K. Tanida *et al.*, Phys. Rev. Lett. **86**, 1982 (2001).
[75] K. Hagino and T. Koike, Phys. Rev. C **84**, 064325 (2011).